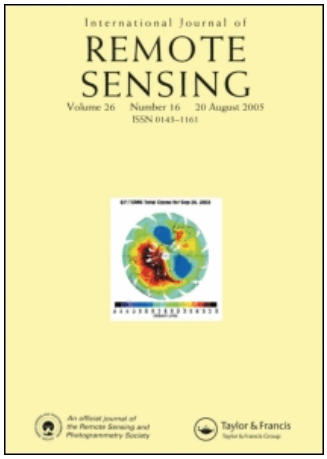

International Journal of Remote Sensing
Publication details, including instructions for authors and subscription information:
http://www.informaworld.com/smpp/title~content=t713722504

High resolution spatio-temporal water vapour mapping using GPS and MERIS observations

Roderick Lindenbergh [a]; Maxim Keshin [a]; Hans van der Marel [a]; Ramon Hanssen [a]
[a] Delft Institute of Earth Observation and Space Systems, Delft University of Technology, 2600 GB Delft, NL

Online Publication Date: 01 April 2008
To cite this Article: Lindenbergh, Roderick, Keshin, Maxim, van der Marel, Hans and Hanssen, Ramon (2008) 'High resolution spatio-temporal water vapour mapping using GPS and MERIS observations', International Journal of Remote Sensing, 29:8, 2393 - 2409
To link to this article: DOI: 10.1080/01431160701436825
URL: http://dx.doi.org/10.1080/01431160701436825

International Journal of Remote Sensing
Vol. 29, No. 8, 20 April 2008, 2393–2409

High resolution spatio-temporal water vapour mapping using GPS and MERIS observations

RODERICK LINDENBERGH*, MAXIM KESHIN, HANS VAN DER MAREL and RAMON HANSSEN

Delft Institute of Earth Observation and Space Systems, Delft University of Technology, P.O. Box 5058, 2600 GB Delft, NL

(*Received 5 May 2006; in final form 8 May 2007*)

Improved knowledge of atmospheric water vapour and its temporal and spatial variability is of great scientific interest for climate research and weather prediction. Moreover, the availability of fine resolution water vapour maps is expected to reduce significant errors in applications using the Global Positioning System, GPS, or radar interferometry. Several methods exist to estimate water vapour using satellite systems. Combining radiances as measured in two spectral bands of the Medium Resolution Imaging Spectrometer (MERIS) results in an Integrated Water Vapor (IWV) product with high spatial resolution, up to 300 m, but a limited temporal resolution of about three days, in case of cloud free conditions. On the other hand, IWV estimates can be derived from the zenith total delays as observed by continuous GPS networks. The GPS IWV estimates have a higher temporal resolution of typically 1 hour, but, even in Western Europe, inter-station distances are at least tenths of kilometres. Here we describe how to obtain IWV products with high spatio-temporal resolution by combining GPS and MERIS IWV estimates. For this purpose an analysis is made of MERIS and GPS based IWV data, retrieved at the same day over Western Europe. A variance–covariance analysis is performed and is subsequently applied to produce time series of combined high-resolution water vapour maps using Kriging. The research presented here is a first step towards near real-time fine resolution water vapour products.

1. Introduction

Water vapour is the atmosphere's dominant greenhouse gas (Cess, 2005; Soden *et al.*, 2005). Besides accounting for a large part of Earth's natural greenhouse effect, gaseous water also condenses to form clouds, which act as an isolation layer for Earth's boundary layer. Knowledge of water vapour values is not only essential for environmental issues but also for satellite measurements from the Global Positioning System (GPS) (Bevis *et al.*, 1992) or (Interferometric) Synthetic Aperture Radar, (In)SAR (Hanssen, 2001). GPS and SAR signals are delayed by water vapour while traversing the atmosphere. Unlike most other atmospheric gases, the distribution of water vapour varies strongly in space and time. The change in IWV above a fixed point at the Earth's surface can to some extent be described by Taylor's frozen flow assumption (Taylor, 1938). This hypothesis states that a random field, in this case the water vapour distribution, is transported as a whole by

*Corresponding author. Email: r.c.lindenbergh@tudelft.nl

International Journal of Remote Sensing
ISSN 0143-1161 print/ISSN 1366-5901 online © 2008 Taylor & Francis
http://www.tandf.co.uk/journals
DOI: 10.1080/01431160701436825

the mean wind. As wind velocities and directions vary with altitude, Taylor's assumption is only of limited use for direct assessment of Integrated Water Vapor values. Elgered *et al.* (2005) show that IWV fields change often significantly within a one-hour period. This makes it necessary to monitor IWV both at high spatial and temporal resolution. Several meteorological and space-geodetic systems exist that can observe IWV, but no single system meets this spatio-temporal resolution requirement (Bevis *et al.*, 1992; Hanssen *et al.*, 1999; Seemann *et al.*, 2003). However, this problem can be overcome by combining IWV observations from suitable complementary systems.

In this paper we consider the fusion of IWV estimates as obtained from the MERIS and GPS satellite systems. At GPS ground stations, the vertically Integrated Water Vapor (IWV) can be derived from the total tropospheric delay that the GPS signals undergo while travelling from the GPS satellites to the ground receivers. This derivation results in relatively accurate IWV estimates with a high temporal (e.g. 1 hour) but a low spatial resolution (tens to hundreds of kilometres). The Medium Resolution Imaging Spectrometer (MERIS) is a push-broom imaging spectrometer with a maximum spatial resolution of 300 m. It measures the solar radiation reflected by the Earth in 15 spectral bands, programmable in width and position, in the visible and near infra-red frequency domain. Although the main mission of MERIS is in oceanography, by observing sea colour, it also observes, amongst others, the water vapour column over land, water or above clouds. Observations are limited to the sun-side of the orbit. MERIS can observe dynamic structures on scales much smaller than possible before. Its temporal resolution however is restricted to three days. MERIS also retrieves cloud type and cloud top height.

Here we analyse MERIS and GPS IWV data over North-West Europe on an arbitrary single day, August 9, 2003. The GPS IWV observations consist of time series of data from 26 ground stations at a temporal resolution of less than an hour. The MERIS data from the same day, acquired shortly after 10 UTC, has a spatial resolution of 1.2 km. The correlation between the two data sources around the acquisition time of the MERIS image is determined by comparing a selected number of MERIS pixels to the GPS IWV estimates. An experimental variance–covariance analysis is performed for both data sets. In the MERIS case this analysis is spatial, in the GPS case it is both spatial and temporal. The two data sets are combined to produce time series of hourly water vapour maps incorporating their spatio-temporal covariances (Goovaerts, 1997; Gneiting *et al.*, 2007). Except for the water vapour maps itself, this procedure results in error maps, displaying the errors as propagated from the individual error components. These results express the expected gain from combining GPS and MERIS water vapour data, provided that there is a reasonably dense network of GPS ground stations, as can be found over e.g. Europe and North America.

2. GPS and MERIS IWV data

2.1 *GPS IWV*

In GPS data processing, measurements from all satellite signal paths are mapped onto the vertical direction by means of a pre-defined mapping function. In this way the effect of GPS path delay in the troposphere can be estimated. This effect is called the zenith tropospheric delay, denoted as D_T. Only the total effect can be directly estimated from GPS measurements in this way, although this is composed of two

components. The zenith hydrostatic delay, D_H, is due to the neutral gases in the troposphere and the non-dipole part of water vapour, while the second component, the zenith wet delay, D_W, appears due to the dipole moment of water vapour. That is,

$$D_T = D_H + D_W. \tag{1}$$

Note that the tropospheric parameters in equation (1) have units of distance, i.e. metres. The zenith hydrostatic delay can be estimated using

$$D_H = 10^{-6} \frac{k_1 R_d P}{g_m} = \frac{0.0022767P}{1 - 0.00266\cos 2\varphi - 2.8 \times 10^{-7} H}, \tag{2}$$

where φ is the ellipsoidal latitude of the GPS station in rad, k_1 an empirical constant [$77.604 \pm 0.014\,\mathrm{K\,mbar^{-1}}$ (Thayer, 1974)], R_d the gas constant of dry air [$461.51\,\mathrm{J\,kg^{-1}\,K^{-1}}$] and g_m the mean gravity in $\mathrm{m\,s^{-2}}$. H indicates the orthometric station height in metres and P the surface air pressure in mbar. The zenith wet delay is then obtained from equation (1) and mapped into integrated water vapour, denoted I and expressed in $\mathrm{kg\,m^{-2}}$, by means of the following expression:

$$Z_W = QI, \tag{3}$$

where Q, a dimensionless quantity, is a function of the mean temperature of water vapour (Klein Baltink *et al.*, 2002).

GPS IWV processing. Zenith tropospheric delay is estimated along with many other parameters, such as station coordinates, etc., by GPS software suites like the Bernese GPS software (Rothacher *et al.*, 1996) and GIPSY-OASIS II (Webb and Zumberge, 1993). This process can be performed both in near real-time and in post-processing mode with time resolutions down to 5–6 min. As every tropospheric estimate typically uses a batch of GPS measurements, the GPS IWV estimates represent in fact a time-averaged amount of water vapour above the receiver location. Numerous validation experiments show that an accuracy of 1–2 $\mathrm{kg\,m^{-2}}$ IWV is achievable for both post-processed and near real-time GPS IWV estimates, see e.g. Jarlemark *et al.* (2002); Klein Baltink *et al.* (2002); Elgered *et al.* (2005). The possibility of using data from GPS networks for operational meteorology has been demonstrated in the framework of the COST-716 project (Elgered *et al.*, 2005), which took place in 2001–2004. In 2003, the period under consideration in this paper, ten European Analysis Centres were participating in that project, which involved processing a network of more than 350 stations covering the whole of Europe.

GPS area of influence. The IWV at a given GPS station at a given time is determined from a number of different signal paths, one for every visible GPS satellite, forming a hypothetical cone, see figure 1. That is, the GPS IWV estimate represents the average of the cross-section of the cone with the effective tropospheric boundary layer height. For the comparison to the MERIS observations, all MERIS pixels within this area of influence (AOI) are averaged. As the configuration of GPS satellites is continuously changing it is at first approach only possible to use an approximate AOI. In this paper we start from a rather simple circular AOI model, which is evidently imperfect. The reasons are twofold. First, GPS IWV estimates represent averaged rather than instantaneous amounts of water vapour. As a consequence, the circular AOI is distorted, e.g. elongated, because of wind-induced water vapour advection. Second, the AOI is affected by the gap in GPS satellite coverage towards the North of GPS ground stations on the Northern hemisphere

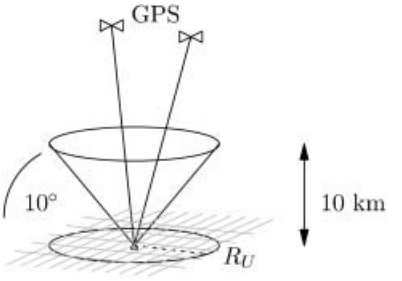

Figure 1. The projected circle indicates the upper bound for the GPS Area of Influence around the GPS ground station at the circle centre, as derived from the cut off angle of 10 deg, combined with a tropospheric height of 10 km. The raster represents the MERIS pixels.

and towards the South on the Southern hemisphere. Note that the area with no GPS satellite visibility in the sky is larger at higher latitudes. Instead of using a fully geometric approach depending on elevation cutoff and signal path geometries, we obtain an optimal radius R_{GPS} as follows. First an upper bound $R_U = 10/\arctan 10 \approx 58$ km for the radius is determined by combining the elevation cutoff angle of 10 degrees with an approximate height of the troposphere, were most water vapour is concentrated, of 10 km. As a measure of agreement between the two types of observations of the IWV, Pearson's correlation coefficient is used. We determine the correlation coefficient between the GPS IWV estimates and the MERIS IWV pixels within a distance R from the GPS stations varying between 0 and the upper bound $R_U = 58$ km in steps of 250 m. The value of R that gives the highest correlation is chosen as the AOI radius R_{GPS}.

2.2 *MERIS IWV*

Here, a short sketch of the MERIS IWV retrieval algorithm is given. More details, together with accuracies, can be found elsewhere, i.e. in Bennartz and Fischer (2001); Fischer and Bennartz (1997). Integrated Water Vapor values are obtained by a differential absorption method from the radiances L_{14} and L_{15} measured in channels 14 and 15, resp. These channels are centred around 885 and 900 nm, with a half width value of ± 10 nm. The ESA algorithm to derive the IWV estimates, W, is based on the logarithmic relation

$$W = k_0 + k_1 \log \frac{L_{15}}{L_{14}} + k_2 \log^2 \frac{L_{15}}{L_{14}}, \tag{4}$$

between the columnar water vapour and the ratio of the spectral radiances from bands 15 and 14. The k_0, k_1 and k_2 are regression constants.

The values of the regression constants depend on the viewing geometry. Moreover, there are also differences in methodology for IWV estimates above land and water. The absorption of water is higher, therefore the aerosol scattering gains influence and is taken into account over water by including the values for the 'aerosol' channels 9, 12, and 13 in the determination of the regression constants. The theoretical accuracy of the estimated water vapour column is $1.7\,\mathrm{kg\,m^{-2}}$ over land and $2.6\,\mathrm{kg\,m^{-2}}$ over water at full resolution. The IWV accuracy at the reduced resolution of 1.2 km is specified to be at most 20% of the IWV estimation.

3. Integrating GPS and MERIS data

3.1 *Spatial and temporal continuity*

As follows from a frozen turbulence hypothesis (Taylor, 1938), local fluctuations of water vapour in the troposphere are transported over a location with a constant wind speed, therefore water vapour measurements obtained at nearby locations and time moments are correlated. Correlation in time or in space between observations can be detected and modelled by a variogram or covariance analysis (Goovaerts, 1997). This model is used to determine the (V)ariance–(C)ovariance matrices of the observations. Using the VC matrices, a Best Linear Unbiased Prediction can be obtained for the IWV content at a given time and location. The underlying assumption used in this framework is that the IWV can be considered as a random function $Z(x, t)$, that is, every observation is one single outcome of a complete distribution of possible observations at location x and at time t.

Given a set of observations, a discrete experimental covariance function is determined by computing experimental covariances between any two observations and by binning the outcomes in distance intervals. The distance intervals should be chosen such that a sufficient number of experimental covariance samples can be found in every bin. By fitting the bin-wise averages of the samples into a positive definite model, a continuous covariance function is obtained that is used to fill the VC-matrix for a prediction at arbitrary location or moment. The obtained spatial, $c_s(x)$, and temporal, $c_t(t)$ covariance functions are combined into a spatio-temporal covariance function $c(x, t)$. The underlying spatio-temporal random function is said to be *separable* (Gneiting *et al.*, 2007), if $c(x, t)$ can be written as

$$c(x, t) = c_s(x)c_t(t) = \frac{c(x, 0)c(0, t)}{c(0, 0)}. \tag{5}$$

Note that a separable covariance function is also *symmetric*, that is $c(x, t) = c(-x, -t)$, for any spatial difference x and any time difference t. Physically, an asymmetric spatio-temporal covariance function can be chosen to implement transport effects due to prevailing wind directions, that is, by incorporating Taylor's frozen flow assumption. Here we adapt the separable case to be used as a starting point, as this is conceptually the easiest. Moreover, thorough comparisons show only a weak dependence of the quality of interpolation results on the type of the spatio-temporal covariance function in case of similar meteo data (Gneiting *et al.*, 2007).

Ordinary Kriging clustering and screening properties. Incorporating the variance–covariance structure of the observations into the interpolation method has two effects that do not occur in case of, e.g. inverse distance interpolation (Wackernagel, 2003; Chilès and Delfiner, 1999). *De-clustering* refers to the partition of weights over correlated observations. The *screening* effect occurs when one observation is behind another observation with respect to the prediction location; the observation behind contains limited new information, and will therefore obtain a low weight compared to the preferred observation in front. It is even possible that the observation behind receives a negative weight. The stress on the weights can be relieved by increasing the so-called *nugget value* or white noise. This value encodes the short time variability or the size of the measurements errors. The clustering and screening effect will have significant influence on the result, especially for the GPS IWV observations which are spatially sparse and not regularly spaced.

3.2 *Spatio-temporal interpolation*

The MERIS IWV observations have a high spatial resolution, but only one epoch of observations is available. On the other hand, the GPS IWV observations are spatially sparse but are available at regular time intervals. Therefore it is straightforward to estimate an IWV value $\hat{I}(t_G, (x, y))$ at time t_G and location $p_0=(x, y)$ as a linear combination

$$\hat{I}(t_G, p_0) = (w_1 I_{G,1}(p_1, t_G) + \cdots + w_n I_{G,n}(p_n, t_G)) + v I_M(p_0, t_M) \tag{6}$$

of GPS IWV observations $I_{G,1}(p_1, t_G)$, …, $I_{G,n}(p_n, t_G)$ made at n different locations at time t_G, and one MERIS IWV observation $I_M(p_0, t_M)$ at location p_0, obtained at time t_M. The weights w_1, …, w_n for the n GPS IWV observations and v for the one MERIS IWV observation are obtained by solving the following ordinary Kriging system.

$$\begin{pmatrix} c(0,0)+N & c(x_{12},0) & \dots & c(x_{1n},0) & c(x_{10},t) & 1 \\ c(x_{12},0) & c(0,0)+N & \dots & c(x_{2n},0) & c(x_{20},t) & 1 \\ \vdots & \vdots & \ddots & \vdots & \vdots & \vdots \\ c(x_{1n},0) & c(x_{2n},0) & \dots & c(0,0)+N & c(x_{n0},t) & 1 \\ c(x_{10},t) & c(x_{20},t) & \dots & c(x_{n0},t) & c(0,0)+N & 1 \\ 1 & 1 & \dots & 1 & 1 & 0 \end{pmatrix} \begin{pmatrix} w_1 \\ w_2 \\ \vdots \\ w_n \\ v \\ \lambda \end{pmatrix} = \begin{pmatrix} c(x_{01},0) \\ c(x_{02},0) \\ \vdots \\ c(x_{0n},0) \\ c(0,t) \\ 1 \end{pmatrix}, \tag{7}$$

where x_{ij} denotes the distance between locations p_i and p_j, and $t=|t_M-t_G|$ the time difference between MERIS and GPS time. N is the nugget. The VC-matrix on the left in equation (7) contains the spatially varying covariances $c(x_{ij}, 0)$ between the GPS IWV observations in the $n \times n$ top left part. Row and column (n+1) contain the spatio-temporal covariances $c(x_{i0}, t)$ between the MERIS observation and the n GPS observations, while the last row and column ensure an unbiased prediction. In the proximity vector on the righthand side, the first n entries contain the spatially varying correlations $c(x_{0i}, 0)$ between the prediction location and the locations of the GPS IWV observations. The $(n+1)$-th entry $c(0,t)$ gives the time-dependent covariance between MERIS observation $I_M(p_0, t_M)$ and the collocated prediction location, while the last entry again is obtained from the unbiasedness condition $w_1+\ldots+w_n+v=1$. The additional nugget, N, on the diagonal of the VC-matrix expresses the uncertainty in the IWV observations. Omitting the nugget in the proximity vector at space-time coincidence of an observation with the prediction is important, because in this case the Kriging system will not simply return the observation as prediction at such a coincidence, a property generally referred to as *exactness*, but will rather divide weight over nearby observations as well, which also results in a more realistic residual error variance value. Solving equation (7) gives a unique solution for the weights, due to the positive definiteness of the VC-matrix.

Except for an IWV prediction $\hat{I}(t_G, p_0)$ we obtain a quality description in the form of a residual variance var(r_0), with $r_0=\hat{I}(t_G, p_0)-I(t_G, p_0)$ the difference between the prediction $\hat{I}(t_G, p_0)$ and the (unknown) real value $I(t_G, p_0)$ of the IWV at the

prediction space-time point, cf.(Goovaerts, 1997; Wackernagel, 2003). The residual variance is given by

$$\mathrm{var}(r_0)_{(t_G,\,p_0)} = c(0,\,0) - \sum_{i=1}^{n} w_i c(x_{0i},\,0) - vc(0,\,t) - \lambda. \tag{8}$$

Basically, the residual variance expresses the proximity, both in space and time, of the observations to the prediction point. The residual variance is minimal at the GPS IWV observation locations and at MERIS acquisition times while it increases with increasing distance, in space and time, between the prediction location and observation locations until no correlation with any of the observations remains. This is illustrated in figure 2 where the mean, minimum, and maximum residual variances per epoch of IWV estimates are given, based on both GPS and MERIS IWV observations. The minimum variance is almost stable at a level of $10\,\mathrm{kg\,m^{-2}}$, reflecting that in each epoch some prediction locations are in the direct vicinity of GPS observations. The mean and maximum variance decreases around the MERIS acquisition time around 10:15 AM to increase again after that. If another MERIS snapshot would be available at, say, 8 PM, again the mean and maximum variance would decrease around that time.

The data fusion procedure as described here is a collocated approach because only the MERIS IWV pixel at the prediction location is taken as an observation. It is fast as the size of the linear system equation (7) is small. The size depends only on the number of GPS ground stations. When interpolating to a map at given GPS epoch time t_G, only the one collocated MERIS observation $I(t_M,\,p_0)$ changes with the prediction location p_0. Therefore only the covariances in row and column $(n+1)$ of the VC-matrix and the first n entries in the proximity vector need to be updated. Disadvantage of such collocated method is that it will not fill any spatial gaps in the MERIS grid. This could be resolved by including a spatial interpolation component for the MERIS observations as well, at the expense of computational efficiency.

4. Data description, comparison and combination

The position of all data considered here is given in WGS84 (World Geodetic System 1984) coordinates. Spherical distances between points are computed along great circles with respect to the WGS ellpisoid. Time is given in Coordinated Universal Time (UTC).

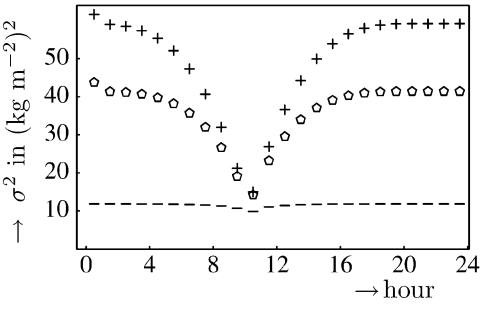

Figure 2. Minimum (dashes), mean (circles) and maximum (pluses) residual error variances per epoch of combined GPS and MERIS IWV estimates.

4.1 *GPS IWV data description*

The GPS data originates from the 26 GPS COST-716 ground stations (Elgered *et al.*, 2005), as shown in figure 3. We used as much data as possible from one processing centre, therefore 24 stations were taken from the GeoForschungsZentrum (GFZ) in Potsdam. Two additional stations processed by the Nordic Geodetic Commission (NKG), were added to improve the spatial coverage. For the given list of stations we consider all available IWV data from August 9, 2003. For the GFZ stations most IWV estimates are available at *h*:15 and *h*:45, where *h* indicates the integer hours, but some data are missing. NKG data is available at 15 minute intervals, but here data points are missing as well.

4.2 *MERIS IWV data description*

We used one MERIS reduced resolution product, acquired at August 9, 2003, between 10:11:27 and 10:14:44 UTC. At reduced resolution, one pixel is available for every $1.2 \times 1.2\,\mathrm{km}^2$ at nadir direction. The MERIS reduced spatial resolution of 1.2 km is much higher than the approximate spatial resolution of 50 km of the GPS IWV estimates at ground stations. Therefore, the reduced MERIS IWV product is suitable to demonstrate the advantages of combining GPS and MERIS IWV data. Further improvements are expected with full resolution (300 m) MERIS IWV data.

Data flags. A MERIS Level 2 data set contains an *Integrated Water Vapor* attribute. The value of this attribute at a given position may not always be representing the actual IWV value, due to, e.g. the presence of cloud cover. Therefore a filter step is necessary. Except for several data attributes, the MERIS Level 2 product also provides a quality attribute by assigning binary 24-bit flags to each product pixel. A unique combination of zeroes and ones addresses the pixel state and quality, according to the classification of the MERIS pixels.

We removed IWV points for which the CLOUD flag, the PCD_14 flag, or the TOAVI_CSI flag is true, see figure 4. The CLOUD flag indicates that the cloud product is available; the PCD_14 flag indicates that the total water vapour content is uncertain, while the TOAVI_CSI flag indicates cloud, snow or ice over land pixels. For our test data set this filter step reduces the number of points in the scene by 20% from 1.25 to 1.09 million points. The other flags were ignored.

4.3 *GPS and MERIS IWV comparison at MERIS time*

Single pixel comparison. After filtering the MERIS data, a comparison was made between the GPS IWV values at the MERIS acquisition time and the values of the remaining MERIS pixels close to the GPS stations. First the MERIS pixel nearest to each of the GPS stations was determined, see figure 5. The correlation between these GPS and MERIS estimates is only 0.63. This relatively low correlation value is mainly caused by some strong outliers. Especially near Stavanger (STAS), Oberpfaffenhofen (OBE2), Pfaender (PFAN) and, to a lesser degree, near Braunschweig (PTBB) and Helgoland (HELG), agreement in estimates is poor. Therefore the MERIS pixels around these GPS stations were considered in detail. In figure 6 the values of the 25 MERIS pixels closest to four such GPS stations are shown: PFAN, HELG, PTBB and STAS. The situation around GPS station OBE2 is not considered, as the nearest MERIS pixel is at a distance of more than 10 km. Around three stations we observe

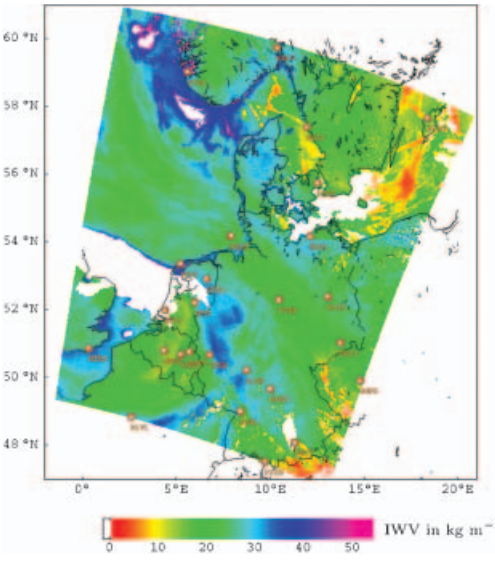

GPS Code	Site Name	Proc. center
APEL	Apeldoorn	GFZ
BRUS	Brussel	GFZ
BUDP	Kbenhavn	GFZ
DELF	Delft	GFZ
DRES	Dresden	GFZ
EIJS	Eijsden	GFZ
EUSK	Euskirchen	GFZ
GOPE	Pecny,Ondrejov	GFZ
HELG	Helgoland	GFZ
HERS	Herstmonceux	GFZ
KARL	Karlsruhe	GFZ
KLOP	Kloppenheim	GFZ
MLVL	Marne-La-Vallee	GFZ
OBE2	Oberpfaffenhofen	GFZ
ONSA	Onsala	GFZ
OEHR	Oehr	GFZ
OSLS	Oslo	NKG
PFAN	Pfaender	GFZ
POTS	Potsdam	GFZ
PTBB	Braunschweig	GFZ
ROST	Rostock-Warnemuende	GFZ
STAS	Stavanger	NKG
TERS	Terschelling	GFZ
VIS0	Visby	GFZ
WARE	Waremme	GFZ
WSRA	Westerbork	GFZ

Figure 3. MERIS water vapour data from August 9, 2003, 10:15 UTC. The MERIS data will be compared and combined with water vapour data from the 26 indicated GPS ground stations.

big discrepancies between neighboring MERIS pixels: in all three cases jumps of more than 5 kg m^{-2} exist. Around STAS a jump from 25.8 kg m^{-2} to 49.8 kg m^{-2} occurs. An explanation for these jumps can be found in the MERIS flags.

Near the PTBB station two single flags, the 'LAND' flag and the 'PCD_19', an aerosol related confidence flag, are true for all pixels and those pixels all have similar values. Around HELG we see more variability in the MERIS pixel values, and in the flags as well. In this case however pixels with similar values not necessarily have identical flags. What should be noted here is that all pixels are marked as 'water', so

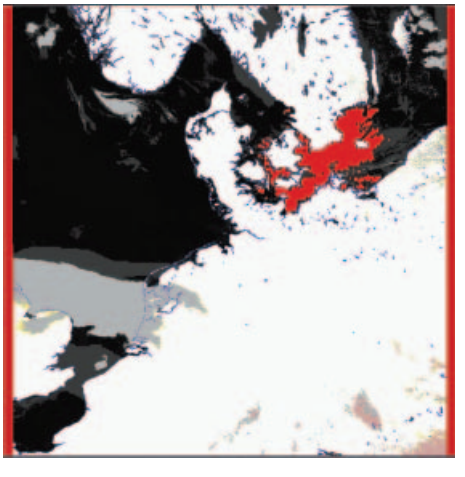

Figure 4. Classification according to MERIS flags. Clearly visible are the land (white), water (black) and coastline pixels (blue). 'Uncertain total water vapour content' is indicated in red, clouds in light grey and 'cloud, snow or ice over land' pixels are in yellow. These pixels were removed from the MERIS data set.

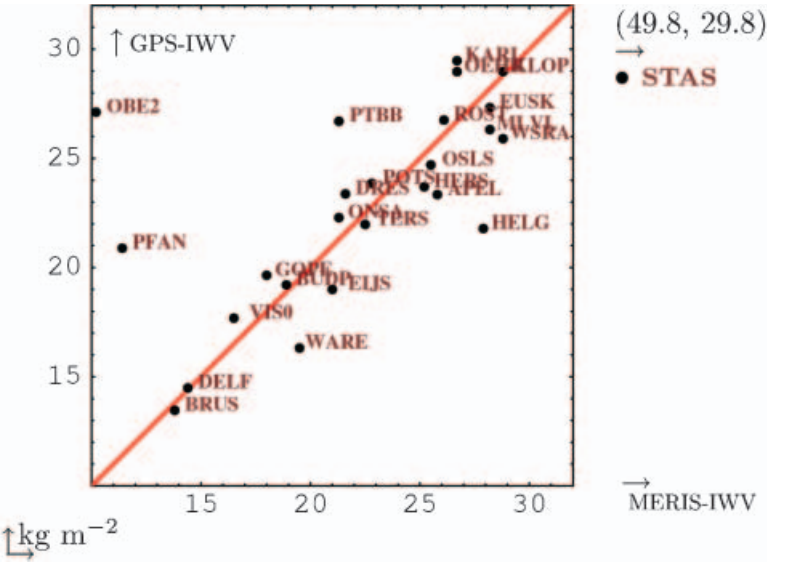

Figure 5. IWV values at GPS stations and at nearest MERIS pixel.

the existence of the two small islands of in total 1.7 km^2 that form Helgoland cannot be recognized on the MERIS image.

Around PFAN we find both 'LAND' and 'WATER' pixels. All MERIS pixels with relative high values are 'LAND' pixels. Intermediate values are found at 'LAND' pixels that are marked as 'COASTLINE' pixels as well. Around STAS the situation is reversed. Here the 'WATER' pixels have high values compared to the 'LAND' pixels. Both in the PFAN and the STAS case the values of the 'LAND' pixels are nearest to the IWV value as determined by the nearby GPS station.

All encountered problems occurred for stations situated near land–water bound aries. Strong jumps in MERIS IWV estimates were observed between neighboring pixels, partly due to different IWV estimations methods used over land and water. Moreover, MERIS pixels exist, e.g. near Helgoland, that are classified as water, although they clearly contain a land component.

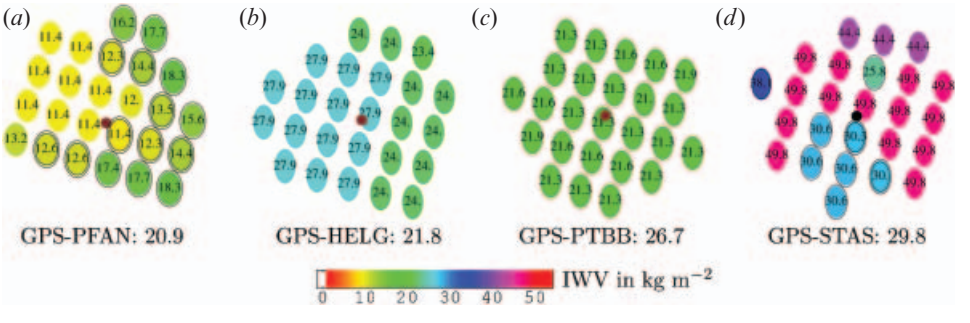

Figure 6. IWV values at 25 MERIS pixels nearest to a GPS station. (*a*) Pfaender; (*b*) Helgoland; (*c*) Braunschweig; (*d*) Stavanger. 'LAND' pixels are surrounded by one circle, 'COASTLINE' pixels by two circles.

Correlation MERIS-GPS vs. GPS area of influence size. After determining the correlation for different AOI sizes of the GPS estimates, as described in §2.1, it is found that the maximum correlation occurs for $R_{GPS}=1.75\,km$. For this AOI of about $10\,km^2$ the GPS-MERIS correlation equals 0.79. Using this radius implies that about 8 MERIS pixels closest to a GPS station are used in the correlation comparison. Note that indeed a maximum in correlation is found inside the interval between 0 km and the upper bound of $R_U=58\,km$, as derived in §2.1.

We discard stations with a maximal absolute difference of more than $5\,kg\,m^{-2}$ between the MERIS pixels within the GPS AOI. In this way the stations of ONSA, PFAN, STAS and TERS (all coastal!) are removed from the comparison because of big jumps, while DELF and OBE2 have no MERIS data to compare within the GPS AOI. For the remaining stations we find a RMS difference of $2.3\,kg\,m^{-2}$, which is comparable to the reported accuracies of the GPS and MERIS IWV observations. A regression analysis yields a Pearson correlation coefficient of 0.85.

4.4 *Experimental spatial and temporal covariance analysis*

GPS spatial correlation. As only 26 GPS stations are considered, it is difficult to determine a reliable covariogram for the spatial correlation at a single epoch. Therefore a spatial experimental covariogram is determined from the, if necessary, linearly interpolated GPS measurements at every hour between 0.30 and 23.30. These times are chosen because most IWV estimates are available at exactly the half hours. The covariogram for 10:30 is shown in dark blue in figure 7(*a*). For the hourly covariograms only those interpolated GPS IWV values are used for which at least one measurement is available within one hour of the covariogram time. The mean of the experimental covariograms obtained in this way is shown in red in figure 7(*a*). This covariogram displays a range, i.e. the maximum distance at which correlation exists, of about 200 km, which agrees for all individual covariograms. The sill or, more precisely, the average experimental covariance within the first bin of 60 km of the individual covariograms, is highly variable during the day, and is on average about 50 $(kg\,m^{-2})^2$. This shows that the size of the spatial covariance of the IWV signal as measured by GPS is highly variable with time, although its range seems more stable.

MERIS spatial correlation. The experimental covariogram of a subset of about 1100 MERIS IWV observations is represented by the dotted line in figure 7(*a*). Here a bin width of 10 km is used. This covariogram is fairly comparable to the covariogram of the GPS IWV data at 10:30. Due to the higher spatial resolution, the range of the MERIS covariogram is higher than the GPS range and is equal to almost 500 km.

GPS temporal correlation. The time series of the GPS IWV at the different GPS ground stations display a strong trend. To ensure second order stationarity, a linear trend was fitted at each station and removed from the data. The mean of the 26 temporal covariance functions determined from the detrended data is given by the brown dots in figure 7(*b*). As the IWV values at most stations even show some non-linear trend during the day, the stationarity condition for an underlying random function does not hold very well. This is expressed by the negative covariance values at higher distances. From the figure it is concluded that the temporal covariance stabilizes after about 10 hours.

4.5 *Optimizing the GPS IWV prediction*

When producing IWV maps from GPS IWV observations, MERIS observations can be used in two different ways. First, MERIS observations can be directly incorporated to produce the water vapour maps as as sketched in §3.2. For this purpose a spatio-temporal covariance function as in equation (5) needs to be determined. Second, the MERIS IWV observations can be used to validate the covariance parameters of the GPS IWV observations.

In order to setup a MERIS reference image, needed for validation of the GPS IWV interpolation, the MERIS observations are resampled to a 0.25×0.1 degree longitude-latitude grid. This implies that one grid cell has an approximate size of 17×11 km. The cell size is small enough to represent local variations in the MERIS signal, and large enough to ensure computational efficiency.

In the following, the resampled MERIS data are used as reference data for optimizing parameters for the interpolation of the GPS IWV data near MERIS time. As a benchmark, the mean absolute difference between the gridded MERIS data and the mean of the GPS IWV observations equals 4.57 kg m^{-2}. Two methods are used for interpolation of the GPS IWV data. For both methods optimal parameter values were determined by minimizing the mean absolute difference at the 0.25×0.1 degree long-lat grid between the resampled MERIS and the interpolated GPS IWV values. First, the GPS IWV observations were interpolated using inverse distance weighting, that is, a weight w_j is assigned to each observation, according to

$$w_j(p) = \frac{1}{\sum_{i=1}^{n} \left(1/d_i^p\right)} \frac{1}{d_j^p}, \tag{9}$$

where n denotes the number of observations and d_j the spherical distance between the interpolation location and the observation. Here the only parameter to determine is the power p of the interpolation. The mean absolute difference reaches its minimum value of 4.06 for $p=3$. The mean absolute difference is determined for different parameters settings within the ordinary Kriging framework as well. Here a minimum absolute difference of 3.90 was obtained with a nugget of zero, a sill of 10, and a range of 3000 km, while using the exponential model. The result of the GPS IWV interpolation using these settings is shown in figure 8(*b*), while figure 8(*c*) shows the difference between the resampled MERIS data and the resulting GPS map.

It is remarkable that the experimental covariance functions as derived in §4.4 indicate a much shorter range than found by the optimization procedure described here. The reason is the often large distance between the interpolation locations and the nearest observations. In such case, ordinary Kriging will not assign a higher weight to the most close observations as these are still beyond the correlation range. As a result, the prediction value will be close to the Kriged mean, that is, the mean which incorporates the correlation between the observations. Due to the use of a long range the Kriging system assigns a higher weight to the nearest observation which leads to better results in the comparison with the MERIS data.

Comparing GPS and MERIS IWV maps. In figure 8 we see MERIS, figure 8(*a*), and GPS, figure 8(*b*), observations interpolated to the same grid at MERIS acquisition time. Clearly, in the MERIS data, small scale features of IWV distribution are

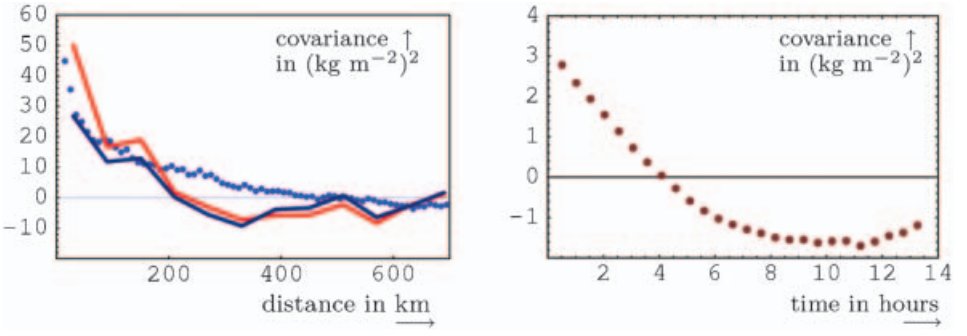

(*a*) (*b*)

Figure 7. Covariograms of the IWV data. (*a*) Spatial – In dark blue: GPS covariogram at 10:30. In red: mean of 24 hourly spatial GPS covariograms. Dotted: covariogram of the MERIS data. (*b*) Temporal – Mean of the 26 temporal covariograms of the detrended IWV values at the different GPS stations.

preserved that are not visible in the interpolated GPS image. It is apparent that the low resolution GPS observations cannot detect fine IWV structure in the spatial domain. This shows the relevance of the use of additional information about spatial IWV distribution, as provided, e.g. by MERIS observations. In the difference picture, figure 8(*c*), green indicates areas for which IWV values are underestimated by the GPS interpolation. In contrary, red indicates areas of overestimation. This figure clearly demonstrates the amount of information that is missed when only using GPS IWV estimates.

4.6 *Spatio-temporal combination*

In this paragraph a first result of the spatio-temporal interpolation procedure as described in §3.2 is presented. In order to produce realistic residual variances of the spatio-temporal estimates, the parameter settings as derived from the spatio-temporal experimental covariance analysis of above are adapted. The common spatio-temporal sill is set to 50 (kg m^{-2})^2. The common spatio-temporal nugget value of 3 (kg m^{-2})^2 reflects the reported GPS and MERIS IWV standard deviations, cf. §2, of 1–2.5 kg m^{-2}. The spatial covariances are taken from an

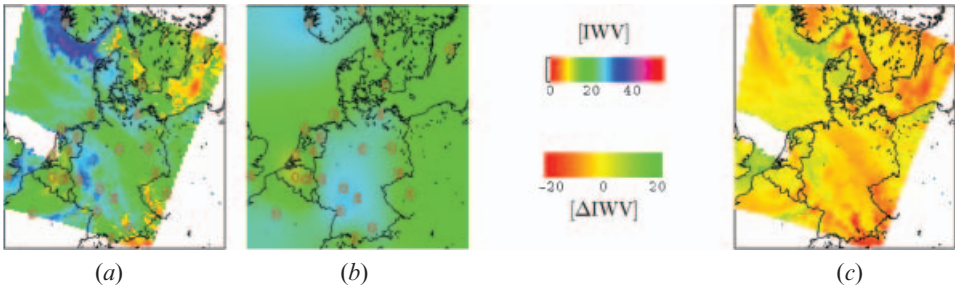

(*a*) (*b*) (*c*)

Figure 8. (*a*) Resampled MERIS, and (*b*) interpolated GPS IWV observations at MERIS time. Both data sets are on the same grid. (*c*) shows the difference between (*a*) and (*b*).

exponentially decreasing model with a range of 500 km. The temporal covariance is modelled by a spherical function with a range of 10 hours.

In figure 9 three epochs of IWV estimates, (*a*)–(*c*), together with their variances, (*d*)–(*f*), are shown. Figures 9(*a*) and 9(*d*) give the estimates and their variances at 10:30 UTC, close to MERIS IWV observation time. Here many small-scale details are visible, having the same pattern as in figure 3, which shows the MERIS IWV observations alone. Nevertheless, it is clear to see that the small-scale details are less profound in the combined estimation map. The variances are low, about 10 $(\mathrm{kg\,m^{-2}})^2$ and homogeneous, as for every estimation location a nearby MERIS IWV observation exists. Figures 9(*b*) and 9(*e*) give the estimates and their variances at 13:30 UTC. Here the GPS IWV observations are dominant at locations where the GPS ground station configuration is more dense, while smaller scale details are visible in regions with sparse GPS information, for example west of Norway. The error variances clearly reflect the availability of the GPS observations: around the GPS stations the variance is minimal and increases with increasing distance to the nearest GPS station until a maximum of about 40 $(\mathrm{kg\,m^{-2}})^2$ is reached. At 18:30 the predicted IWV distribution, figure 9(*c*), is very smooth because it is by now

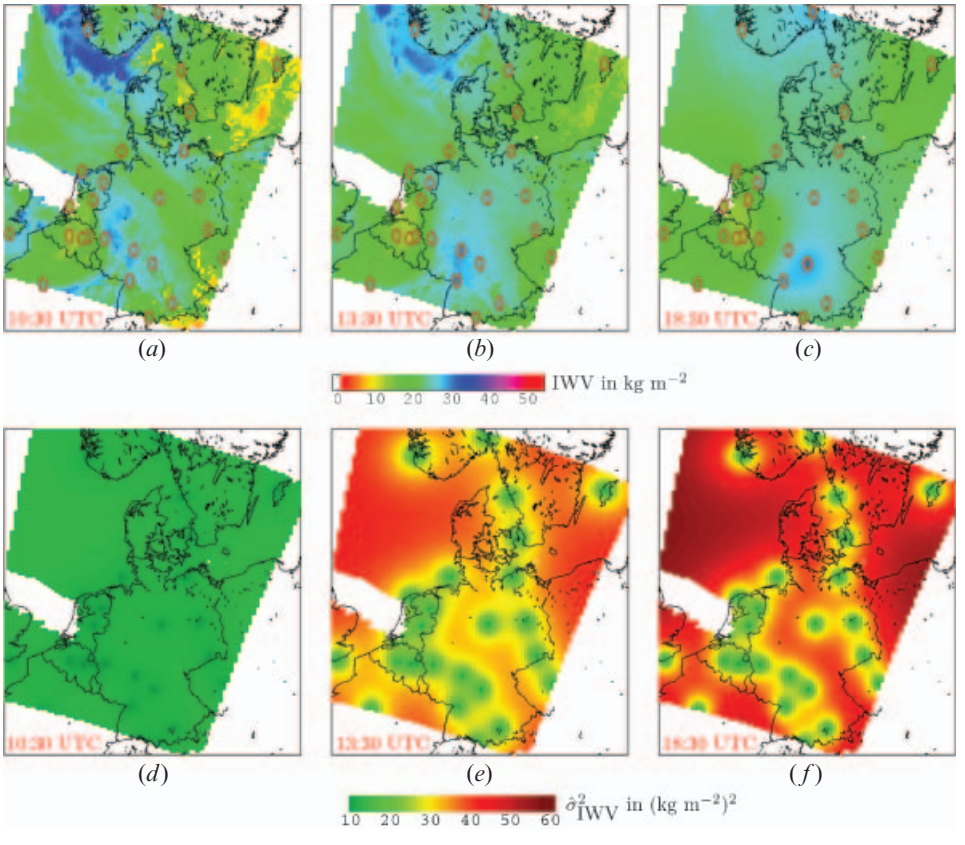

Figure 9. Top: maps of the IWV contents over North-West Europe at August 9, 2003: (*a*) at 10:30 UTC; (*b*) at 13:30 UTC and (*c*) at 18:30 UTC, obtained by combining IWV observations from MERIS and GPS. Bottom: residual variances of the IWV contents for (*a*), (*b*) and (*c*) respectively.

completely driven by the GPS IWV observations, as there is no temporal correlation anymore with the MERIS acquisition.

The variances, figure 9(*f*), show the same pattern as at 13:30 UTC, but are larger, especially in regions further away from the GPS stations, as the lack of temporal correlation with the MERIS image is the most influential on the variance at locations where also the spatial correlation with the GPS observations is low. Note that an overview of the development of the minimum, mean and maximum error variances during the day is already given in figure 2. The variance maps clearly show that acceptable combined spatio-temporal estimations can only be achieved when the spatio-temporal availability of GPS and MERIS IWV estimates is good enough. As only a part of the operational GPS ground stations were used in this research, the optimal possible situation, especially over European land area, is much better than demonstrated here.

5. Conclusions and further research

In this paper we present the results of a spatio-temporal combination of GPS and MERIS IWV observations. The combination is performed by solving an ordinary Kriging system with suitable spatio-temporal covariances between MERIS and GPS measurements. For this purpose we used GPS IWV data from 26 GPS ground stations and a MERIS image acquired at a nearly cloudless day in 2003. As a first step GPS and MERIS IWV data from the same time and location were compared in order to assess the consistency of the IWV estimates from both the systems.

We found a correlation of 0.85 and a RMS difference of $2.3\,\mathrm{kg\,m^{-2}}$ when comparing an IWV observation at a GPS station with the average of the MERIS IWV pixels within a circle with optimal radius of 1.75 km. Coastal stations with a jump between neighboring MERIS IWV pixel values of more than $5\,\mathrm{kg\,m^{-2}}$ within the GPS area of influence were removed. Such jumps, far beyond the specified accuracy, typically occurred near coastline GPS stations, because the MERIS IWV algorithm uses different methods above land and water. A further analysis of near-coastal IWV values may lead to an improvement of the current algorithms as used by MERIS for processing IWV data. The resulting correlation value shows that the reported accuracies of the MERIS and GPS IWV observations are consistent.

The spatially dense MERIS IWV observations can be used as reference data to find optimal parameter values for the spatial interpolation of the GPS IWV observations. In this way a much longer correlation range is found than that provided by the experimental covariance function analysis. The first results of a spatio-temporal combination of the GPS and MERIS IWV observations match the intuition. Moreover, the estimated residual error variances give a quality description of the combined IWV product at a given time and location. One known problem with this type of variance however is that it only depends on data configuration rather than on data values. In case of pixel jumps, one might obtain too optimistic variance estimates. An alternative approach for assessing local uncertainty is to simulate many possible realizations of the IWV distribution and to consider the variability in the outcomes at a given time and location (Goovaerts, 1997). This computationally more elaborated approach is expected to provide realistic variance estimates, even in case of jumps.

A next step of this research will be to incorporate wind data in the spatio-temporal combination, as, according to Taylor's frozen flow assumption, wind transports water vapour fields as a whole, albeit to a limited temporal extent.

Another necessary extension, especially when considering IWV estimates over mountainous areas, is to include topographic height information in the spatio-temporal interpolation of the GPS and MERIS IWV observations. It is well-known that the IWV content decreases exponentially with increasing topographic elevation. Therefore, heights from a suitable digital elevation model, e.g. ESA's GETASSE30 30 arc second resolution product (Brockmann *et al.*, 2006), should be incorporated in the interpolation. Two different procedures demonstrate such approach for the spatial interpolation of GPS IWV data alone, one over Switzerland (Morland and Mätzler, 2007), where observations were normalized to a standard height of 500m, and one over Italy (Basili *et al.*, 2004), where heights were added to a Kriging system by means of a deterministic external drift.

The first results, as presented in this paper, were obtained with one day of observations only. Future research will focus on one month of consecutive MERIS IWV images together with high resolution GPS IWV time series. Testing data covering larger time intervals will allow for more adequate validation procedures. This will demonstrate the possible benefit from incorporating, e.g. topography and wind information. Comparing predictions one hour ahead with real measurements will allow for better gauging of the spatio-temporal interpolation parameters. This will lead to an adequate quality description of the combined MERIS-GPS water vapour estimates. Given a sufficient number of GPS stations, this procedure will result in a high quality near real-time, spatially dense water vapour product to be used in numerical weather forecast models as well as in various applications using (In)SAR and GPS/Galileo.

Acknowledgments

We would like to thank Sybren de Haan from the Dutch Royal Meteorological Society, KNMI for providing the authors with the GPS IWV data as well as for his useful comments. The MERIS data used in this paper are disseminated by the European Space Agency, ESA. This project is funded under number EO-085 by the Netherlands Institute for Space Research, SRON. Finally we would like to express our thanks to the three anonymous reviewers who provided us with many valuable comments and advice.

References

Basili, P., Bonafoni, S., Mattioli, V., Ciotti, P. and Pierdicca, N., 2004, Mapping the atmospheric water vapor by integrating microwave radiometer and GPS measurements. *IEEE Transactions on Geoscience and Remote Sensing*, **42,** 8, pp. 1657–1665.

Bennartz, R. and Fischer, J., 2001, Retrieval of columnar water vapour over land from back-scattered solar radiation using the Medium Resolution Imaging Spectrometer (MERIS). *Remote Sensing of Environment*, **78**, pp. 271–280.

Bevis, M., Businger, S., Herring, T., Rocken, C., Anthes, R. and Ware, R., 1992, GPS Meteorology: remote sensing of atmospheric water vapor using the global positioning system. *Journal of Geophysical Research*, **97**, pp. 15787–15801.

BROCKMANN, C., 2006, BEAM Version 3.6 – The Basic ENVISAT Toolbox for MERIS, (A)ATSR and ASAR. http://www.brockmann-consult.de/beam, Last visited: January 16, 2007.

CESS, R.D., 2005, Water vapor feedback in climate models. *Science*, **310,** 5749, pp. 795–796.

CHILÈS, J.-P. and DELFINER, P., 1999, *Geostatistics: modeling spatial uncertainty.* Wiley Series in Probability and Statistics (New York: John Wiley, 1999).

ELGERED, G., PLAG, H.-P., VAN DER MAREL, H., BARLAG, S. and NASH, J., 2005, Exploitation of ground-based GPS for operational numerical weather prediction and climate applications, Final report. Technical Report, COST Action 716, European cooperation in the field of scientific and technical research.

FISCHER, J. and BENNARTZ, R., 1997, Retrieval of total water vapour content from MERIS measurements, Algorithm theoretical basis document. Technical Report PO-TN-MEL-GS-0005, ESA-ESTEC, Noordwijk, Netherlands.

GNEITING, T., GENTON, M.G. and GUTTORP, P., 2007, Geostatistical space-time models, stationarity, separability and full symmetry. In *Statistical Methods for Spatio-Temporal Systems*, B. Finkenstadt, L. Held and V. Isham (Eds) (Boca Raton: Chapman & Hall/CRC, 2007), pp. 151–175.

GOOVAERTS, P., 1997, *Geostatistics for Natural Resources Evaluation* (New York: Oxford University Press, 1997).

HANSSEN, R.F., 2001, *Radar Interferometry* (Dordrecht: Kluwer Academic Publishers, 2001).

HANSSEN, R.F., WECKWERTH, T.M., ZEBKER, H.A. and KLEES, R., 1999, High-resolution water vapor mapping from interferometric radar measurements. *Science*, **283,** 5406, pp. 1297–1299.

JARLEMARK, P., JOHANSSON, J., STOEW, B. and ELGERED, G., 2002, Real time GPS data processing for regional atmospheric delay. *Geophysical Research Letters*, **29,** 16, pp. 7/1–4.

KLEIN BALTINK, H., VAN DER MAREL, H. and VAN DER HOEVEN, A.G.A., 2002, Integrated atmospheric water vapor estimates from a regional GPS network. *Journal of Geophysical Research*, **107**, pp. 3.1–3.8.

MORLAND, J. and MÄTZLER, C., 2007, Spatial interpolation of GPS integrated water vapour measurements made in the Swiss Alps. *Meteorological Applications*, **14**, pp. 15–26.

ROTHACHER, M., BEUTLER, G., BROCKMANN, E., FANKHAUSER, S., GURTNER, W., JOHNSON, J., MERVART, L., SCHAER, S., SPRINGER, T. and WEBER, R., 1996, The Bernese GPS Software Version 4.0. Technical Report, Astronomical Institute, University of Berne, Switzerland.

SEEMANN, S.W., LI, J., MENZEL, W.P. and GUMLEY, L.E., 2003, Operational retrieval of atmospheric temperature, moisture, and ozone from MODIS infrared radiances. *Journal of Applied Meteorology*, **42**, pp. 1072–1091.

SODEN, B.J., JACKSON, D.L., RAMASWAMY, V., SCHWARZKOPF, M.D. and HUANG, X., 2005, The radiative signature of upper tropospheric moistening. *Science*, **310,** 5749, pp. 841–844.

TAYLOR, G.I., 1938, The spectrum of turbulence. *Proceedings Royal Society London, Series A*, **164**, pp. 476–490.

THAYER, G., 1974, An improved equation for the radio refractive index of air. *Radio Science*, **9**, pp. 803–807.

WACKERNAGEL, H., 2003, *Multivariate Geostatistics*, 3rd edn (Berlin: Springer, 2003).

WEBB, F. and ZUMBERGE, J., 1993, An introduction to GIPSY/OASIS-II. Technical Report D-11088, Jet Propulsion Laboratory, Pasasena, California.